Journal of Natural Fibers

ISSN: 1544-0478 (Print) 1544-046X (Online) Journal homepage: www.tandfonline.com/journals/wjnf20

High Velocity Impact Response and Damage Analysis of Hybrid Aluminum/Carbon Fiber/ Pineapple Leaf Fiber Laminates for Automotive Structure Using TOPSIS Method

Hanyue Xiao, Mohamed Thariq Hameed Sultan, Farah Syazwani Shahar, Suhas Yeshwant Nayak, Muhammad Imran Najeeb, Siti Madiha Muhammad Amir & Sapizah Rahim

To cite this article: Hanyue Xiao, Mohamed Thariq Hameed Sultan, Farah Syazwani Shahar, Suhas Yeshwant Nayak, Muhammad Imran Najeeb, Siti Madiha Muhammad Amir & Sapizah Rahim (2025) High Velocity Impact Response and Damage Analysis of Hybrid Aluminum/ Carbon Fiber/Pineapple Leaf Fiber Laminates for Automotive Structure Using TOPSIS Method, Journal of Natural Fibers, 22:1, 2445583, DOI: 10.1080/15440478.2024.2445583

To link to this article: https://doi.org/10.1080/15440478.2024.2445583

JOURNAL OF NATURAL FIBERS
2025, VOL. 22, NO. 1, 2445583
https://doi.org/10.1080/15440478.2024.2445583

High Velocity Impact Response and Damage Analysis of Hybrid Aluminum/Carbon Fiber/Pineapple Leaf Fiber Laminates for Automotive Structure Using TOPSIS Method

Hanyue Xiao[a,b], Mohamed Thariq Hameed Sultan [a,c,d], Farah Syazwani Shahar[a], Suhas Yeshwant Nayak[e], Muhammad Imran Najeeb[f], Siti Madiha Muhammad Amir[g], and Sapizah Rahim[g]

[a]Department of Aerospace Engineering, Faculty of Engineering, Universiti Putra Malaysia, Serdang, Selangor Darul Ehsan, Malaysia; [b]School of Intelligent Manufacturing and Automobile, Chongqing College of Electronic Engineering, Chongqing Polytechnic University of Electronic Technology, Chong Qing, China; [c]Laboratory of Biocomposite Technology, Institute of Tropical Forestry and Forest Products (INTROP), Universiti Putra Malaysia, Serdang, Selangor Darul Ehsan, Malaysia; [d]Aerospace Malaysia Innovation Centre (944751-A), Prime Minister's Department, MIGHT Partnership Hub, Cyberjaya, Selangor Darul Ehsan, Malaysia; [e]Department of Mechanical and Industrial Engineering, Manipal Institute of Technology, Manipal Academy of Higher Education, Manipal, Karnataka, India; [f]Department of Engineering Education, Faculty of Engineering and Built Environment, Universiti Kebangsaan Malaysia, Bangi, Malaysia; [g]Industrial Technology Division, Malaysian Nuclear Agency, Kajang, Selangor, Malaysia

ABSTRACT

With the rising demand for lightweight and high-performance materials in automotive applications, this study examines the high-velocity impact (HVI) behavior and damage mechanisms of fiber metal laminates (FMLs) composed of aluminum (A), carbon fiber (C), and pineapple leaf fiber (P). Using the Technique for Order Preference by Similarity to the Ideal Solution (TOPSIS), we identified the optimal FMLs from four layer sequences (APPPA, ACPCA, APCPA, and CPAPC). The best-performing FML, ACPCA, was tested at various impact velocities (73.33 m/s, 86.08 m/s, 92.33 m/s, 101.35 m/s, 132.96 m/s, and 144.27 m/s). Damage modes and failure were analyzed through visual inspection, infrared thermography (IR), radiography testing (RT), and scanning electron microscopy (SEM). Results showed that the ACPCA specimen absorbed all impact energy up to 92.33 m/s without complete perforation but was fully penetrated at higher velocities. The highest energy absorption recorded was 29.74 J at 132.96 m/s, with a specific energy absorption (SEA) of 76.49%. Given their exceptional energy absorption capabilities, hybrid FMLs demonstrate excellent potential for automotive applications, such as door panels, roof structures, bumpers, and vehicle armor, where impact resistance, durability, and lightweight properties are critically important.

摘要

随着汽车应用对轻质高性能材料需求的增加，本研究考察了由铝（A）、碳纤维（C）和菠萝叶纤维（P）组成的纤维金属层压板（FML）的高速冲击（HVI）行为和损伤机制. 使用与理想解相似性排序偏好技术（TOPSIS），我们从四个层序列（APPPA、ACPCA、APCPA和CPAPC）中确定了最佳FML. 在各种冲击速度（73.33 m/s、86.08 m/s、92.33 m/s、101.35 m/s、132.96 m/s和144.27 m/s）下测试了性能最佳的FML ACPCA.

KEYWORDS

Pineapple leaf fiber; fiber metal laminates; TOPSIS; high velocity impact test; automotive application

关键词

菠萝叶纤维; 纤维金属层压板; 高速冲击试验; 汽车应用

CONTACT Mohamed Thariq Hameed Sultan thariq@upm.edu.my Department of Aerospace Engineering, Faculty of Engineering, Universiti Putra Malaysia, 43400 UPM Serdang, Selangor Darul Ehsan, Malaysia; Suhas Yeshwant Nayak suhas.nayak@manipal.edu Department of Mechanical and Industrial Engineering, Manipal Institute of Technology, Manipal Academy of Higher Education, Manipal, Karnataka 576104, India

通过目视检查、红外热成像（IR）、射线检测（RT）和扫描电子显微镜（SEM）分析了损伤模式和故障. 结果表明，ACPCA试样吸收了高达92.33 m/s的所有冲击能量，没有完全穿孔，但在较高速度下完全穿透. 记录的最高能量吸收为29.74　J，速度为132.96 m/s，比能量吸收率（SEA）为76.49%. 鉴于其卓越的能量吸收能力，混合动力FML在汽车应用中展现出巨大的潜力，如门板、车顶结构、保险杠和车辆装甲，在这些应用中，抗冲击性、耐用性和轻质性至关重要.

Introduction

In the automobile industry, manufacturers have been exploring lightweight materials to meet fuel economy standards and customer demands, driven by emission reduction regulations and energy-saving strategies (Khalid et al. 2021). FMLs represent a typical hybrid material offering significant advantages in performance and weight reduction compared to traditional metallic automotive materials. FMLs combine ductile metal layers with high-strength synthetic fiber-reinforced polymer (FRP) layers, providing superior mechanical properties such as enhanced damage tolerance and impact resistance, crucial for both aerospace and automotive applications (Ding et al. 2021; Vasiliev and Morozov 2018). In addition, a rising awareness of the sustainable development has prompted increased interest in eco-friendly automotive materials (Mattsson, Hansson, and Cedervall 2015; Wang et al. 2020). Consequently, this heightened ecological consciousness has encouraged researchers to explore alternative sources of natural fibers as substitutes for synthetic fibers in FRP composites because of their outstanding properties, including low density, abundant availability, cost-effectiveness, ease of processing, and biodegradability. Depending on their origin, natural fibers are categorized as animal fibers or plant fibers, the latter primarily composed of cellulose, hemicellulose, lignin, pectin, wax, and moisture. There are many types of natural fibers include cotton, flax, hemp, pineapple leaf, jute, etc., used as reinforcements in polymer matrices. Studies have demonstrated that natural fibers hold significant promise for use in natural fiber metal laminates composites (NFMLs) and as replacements to artificial fibers (Germano et al. 2023; Ng et al. 2023). Researchers have shown that certain NFMLs materials can achieve comparable mechanical performance to traditional materials with the added benefit of reduced weight and environmental sustainability (Sahu and Gupta 2020; Selvaraj, Maneengam, and Sathiyamoorthy 2022; Vinod, Sanjay, and Siengchin 2023).

However, single fiber has their own limitations, such as the high price and non-biodegradable of synthetic fibers, and the lower environment resistance of natural fibers. To mitigate these effects, hybridization is a considerable method that would minimize their drawbacks, combines their advantages, improves the fiber – matrix bonding, and enhances material stability under varying environmental conditions (Dadej and Bieniaś 2020; Ravi et al. 2022). Numerous studies have shown that hybrid synthetic fibers with abundantly available natural fibers offer superior properties compared to single fiber composites. Murugu et al. (2021), showed that hybrid glass fiber (GF)/hemp fiber (HF) reinforced polymers can be utilized for automobile body materials, exhibiting greater impact performance than single GF-reinforced composites, potentially reducing harm to drivers in accidents. H. Xiao et al. (2023) hybrid pineapple leaf fiber (PALF) with carbon fiber (CF) into FMLs, finding that the hybrid composites have intermedium mechanical performance between fully C-reinforced composite and fully P-reinforced composites. Chee et al. (2019) developed hybrid composites using bamboo, kenaf, and epoxy. Their findings indicated that a 50:50 blend of bamboo and kenaf provided a fair mix of environmental impact resistance and biodegradability. Bisheh (2024) explored hybrid combinations of bamboo fiber (BF) with Kevlar fiber (KF), CF, and/or GF for automotive shafts, concluding that hybrid bio/synthetic fiber-reinforced composites provided better solutions meeting design criteria with lower weight and cost for automobile components. Specifically, BF/CF hybrids led to the lightest structures when lightweight was paramount, and hybrid BF/GF results in the cheapest

structures if the cost is the primary consideration. In total, these studies indicate that hybrid fibers can alleviate the limitations of single fibers by balancing the mechanical performance, environmental resistance, biodegradability, and cost that can be widely used in various applications, such as aerospace, automotive, shipping, and so on (Ahmadijokani et al. 2020; Lawrence, Oguamanam, and Bougherara 2022).

Impact test is indispensable for automotive materials to ensure they can withstand severe forces and maintain structural integrity, ultimately enhancing safety and reliability. FMLs usually display excellent impact resistance because of the combination of ductile metal layers and high-strength FRP composites (Olhan, Khatkar, and Behera 2022; Sharma et al. 2021; Vieira et al. 2022). HVI testing is a typical method to evaluate the materials performance under intense and rapid impacts, such as those encountered during ballistic events or severe crashes. These tests involve striking a specimen with high-speed bullets or impactors to simulate extreme conditions. The primary focus of HVI testing is to assess the material's ability to absorb and dissipate energy, as well as its resistance to penetration or fracture under high-velocity impacts. HVI on composites generally occurs at velocities above 10 $m.s^{-1}$. Such impacts can cause extensive visible damage and even complete destruction of the component. Penetration by HVI bullets can cause the immediate injury or death of crewmembers due to the kinetic energy of their fragments, heat, light flash, and over-pressurization. Meanwhile, low-velocity impacts below 10 $m.s^{-1}$ which may generally occur during maintenance or servicing of components, may go unnoticed due to the microscopic nature of damage (Stephen et al. 2022). Such barely visible impact damage causes severe deterioration to the strength and impact resistance of composites and thus, it is necessary to be investigated along with the HVI behavior of the composites.

After mechanical testing, observing specific types of damage mechanism is vital while determining the mechanical properties of the hybrid bio/synthetic FMLs. For FMLs, one of the failure mechanisms is presented as delamination. Many researches have shown that the primary reason for FMLs failure is the delamination between the metal and FRP layers (Gardner et al. 2022; Khan and Sharma 2022). The service life of composite structures is often limited by delamination, which lowers their stiffness and strength. Inter-layer delamination is another common type of damage experienced by laminate composites (Monetto 2019). The displacement of broken and undamaged fibers and interlaminar cracks results in inter-layer debonding between adjacent plies (Vasiliev and Morozov 2018). Additionally, matrix crack is also a critical factor affecting the results of composite materials' failure (Chiachío et al. 2016). Matrix crack occurs when the stress on the material surpasses the threshold, causing the matrix material between the fibers to break or causing fibers to separate from the matrix. Matrix microcracks may also trigger global delamination zones around the free edges of the quasi-isotropic or angle-ply laminates (Zubillaga et al. 2015). Besides delamination and matrix crack, researches have shown that composites may also experience fiber failure (pull-out and breakage) after tensile and impact testing (Najeeb et al. 2021). Damages start from fiber fracture, causing stretching along with bending, and ultimately leading to fiber failure.

There already have a lots of researches on the HVI behavior of FMLs, and the impact resistance varies depending on factors such as fiber/matrix type, layering sequence, layer thickness, and interfacial bonding (Andrew et al. 2019). Liu, Zhang, and Ye (2017) studied the HVI properties of sandwich structured materials with an aluminum (Al) foam core and outer FMLs layers made by Al sheets and woven GF layer. They found that increasing the thickness of the outer FMLs layers significantly improves the energy absorption of the composite. Sharma et al. (2021) studied the HVI performance of titanium (Ti)/GF FMLs, emphasizing the critical role of metal layer thickness, with thicker metal layers displaying greater crack resistance than other FMLs. At impact energies of 30 J and 90 J, FMLs [Ti/GF/Ti/GF_2/Ti/GF/Ti] with 0.3 mm Ti layers showed 30% and 10% higher damage degree than FMLs [Ti/GF_4/Ti] with 0.6 mm metal layers, respectively. Sangsefidi et al. (2021) studied the HVI performance of sandwich-structured FMLs Al/GF/Al with different numbers of FRP layers, and they found that increasing the number of FRP plies led to greater permanent deformation of non-rigid projectiles. Furthermore, the amount of crushing failure, fiber breakage, debonding and delamination area, and permanent deformation of the rear

aluminum facing plate also considerably increased with the increased layers. In addition, some studies have explored the influence of bullet types used in HVI testing. Q. Zhu et al. (2019) researched the ballistic performance and damage characteristics of FMLs reinforced by Al/CF under HVI with different bullets shapes. They identified principal failure mechanisms such as shear failure on the front Al layer, tensile failure on the back Al layer, and both tensile and shear fiber failures in the FRP when using flat-headed bullets. Sharp-nosed bullets, similar to hemisphere-nosed bullets, resulted in plug formation on the front Al layer, with predominant extrusion tensile failure on the back, accompanied by some fiber breakage and debris.

According to these researches, selecting the best laminate from the available resources is a challenge because of the numerous factors influencing FMLs, such as material types, composite structures, layer sequences, hybridization, manufacturing processes, density, and cost. Thus, various analytical methods are recommended to facilitate appropriate materials selection. The TOPSIS is a powerful multi-criteria decision analysis method developed by Hwang and Yoon in 1981 (Abdel-Basset et al. 2024). It is premised on the concept that the optimal alternative is the one that falls closest to the Positive Ideal Solution (PIS) and furthest from the Negative Ideal Solution (NIS) (Nadeem et al. 2023). These ideal solutions encapsulate the best and worst values of achievable criteria, respectively. In the realm of decision-making tools, TOPSIS distinguishes itself through its systematic approach in assessing alternatives based on a multitude of attributes, thereby generating a comprehensive score for each alternative. Several key attributes contribute to its prominence, including its rapid identification of the best alternative, computational efficiency, and the capacity to quantitatively measure the relative performance of each alternative. Furthermore, TOPSIS provides flexibility in defining the choice set and its computational process is simple enough to be easily integrated into a spreadsheet. Its logical framework mirrors the human decision-making rationale, particularly beneficial in intricate decision scenarios like material selection (Jha et al. 2022). It enables a holistic view where the influence of each attribute is considered in relation to others, allowing for direct or inverse compensation of one attribute by others (Almomani et al. 2024; Arredondo-Galeana et al. 2023; Pang et al. 2024). Consequently, this integrated approach makes TOPSIS a suitable technique for complex multi-criteria material selection.

This research contributes to the field by introducing a simple approach to the design and selection of FMLs, conducting comprehensive evaluations of their HVI behavior for automotive applications. Specifically, we integrated the TOPSIS to methodically select the optimal stacking sequence from four configurations of FMLs Al/CF/PALF. This selection aims to balance lightweight properties and mechanical performance, considering critical factors including density, hardness, tensile, flexural, ILSS, and Izod. The selected hybrid FMLs underwent HVI testing, and the visual inspection, non-destructive test (NDT) including infrared thermography (IR), radiographic testing (RT), and scanning electron microscopy (SEM) were used to observe the damage behavior. The previously unexplored hybrid FMLs Al/CF/PALF not only offer promising mechanical performance but also present new possibilities for applications in the automotive industry, as it incorporates PALF which are lightweight, eco-friendly, and biodegradable.

Materials and experimental methods

Materials

Aluminum 6061 – T6 sheets with 0.4 mm thickness were supplied by Mechasolve Engineering Company (MSEB). The circular holes of diameter 1 mm were drilled in an Al sheet at a pitch distance of 75 mm by water jet cutting. Given that anodizing can remarkably enhance the adhesion between the Al and FRP layers, the Al sheets were systematically subjected to mechanical exposure, alkaline etching, and anodizing to establish robust interfacial bonding between the Al and FRP layers (Khalid, Rashid, and Sheikh 2021). The woven PALF fabric and unidirectional CF fabric were also sourced from MESB, with an areal density of 315 gsm and 210 gsm, respectively. The set of epoxy resin

(EpoxAmiteTM 100 and the slow hardener EpoxAmiteTM 103) was provided by Smooth-On company. The slow-curing hardener is used to ensure thorough resin impregnation and to mitigate thermal stresses and potential material distortion during the VARTM process.

FMLs fabrication

By use of the VARTM process, the selected FMLs were manufactured into a size of 300 × 300 mm. The VARTM setup included a mold, sealant tape, a peel ply, an infusion mesh, a vacuum bag, a resin container, a vacuum pump, an intake and outlet tube. After cleaning the surface of the glass mold with acetone to remove impurities and debris, three coatings of wax were applied to the mold and allowed to cure for at least 20 minutes before being wiped off. Following that, the hybrid layers were put on the mold in the design order, followed by a layer of peel ply and another layer of infusion mesh over the materials. Finally, the VARTM mold is sealed with a flexible polyethylene vacuum bag that covers the plies. The resin infusion procedure was started by mixing the epoxy and the hardener in a 100:28.4 weight ratio. When the resin is ready, it is immediately transported inside the resin storage tank and linked to the inlet tube for resin infusion. The composite curing procedure takes least 24 hours at room temperature.

Topsis method

TOPSIS method is used to assign ranks to samples according to the criteria (performance) score of the data. The criteria for the materials selection, from the finest to the worst materials, have been created for automotive applications. By using TOPSIS method, materials will be analyzed and ranked accordingly, and then the materials are prioritized based on TOPSIS method ranking, so that best and suitable material can be identified. The TOPSIS solution technique includes the subsequent steps (Chee et al. 2019; Ding et al. 2021; Mattsson, Hansson, and Cedervall 2015; Sahu and Gupta 2020):

Step 1: Formulate a decision matrix according to the criteria for the ranking. The typical matrix format is shown as the following:

$$D = \begin{array}{c} \\ A_1 \\ A_2 \\ \vdots \\ A_m \end{array} \begin{array}{c} \begin{array}{cccc} C_1 & C_2 & \cdots & C_n \end{array} \\ \begin{bmatrix} x_{11} & x_{12} & \cdots & x_{1n} \\ x_{21} & x_{22} & \cdots & x_{2n} \\ \vdots & \vdots & \vdots & \vdots \\ x_{m1} & x_{m2} & \cdots & x_{mn} \end{bmatrix} \end{array} \tag{1}$$

Where A_1, A_2, ., A_m are the viable alternatives from which the decision makers have to choose, C_1, C_2, ., C_n are the criteria by which the alternative performance is measured, X_{ij} is the qualification of the alternative A_i with respect to the criterion C_j.

Step 2: Normalization standardizes the values across different criteria, preventing biases due to different measurement scales or units. This ensures that each criterion contributes equally to the evaluation process. Normalize the given decision matrix according to the following Equation 2.

$$n_{ij} = \frac{r_{ij}}{\sqrt{\sum^{i=1} mr_{ij}^2}}, \mathrm{i} = 1, 2, \ldots .\mathrm{m}, \mathrm{j} = 1, 2, \ldots .\mathrm{n}. \tag{2}$$

Step 3: Weighted normalized decision matrix: After normalization, the weighted decision matrix incorporates the relative importance or weight of each criterion in the decision-making process. The weight criteria (W_j) associated with each column determine the importance of the weights of the attributes. This research utilized the mean weight method as Equation 3 (Ardil 2021). The mean weight is based on the assumption that all criteria are of equal importance when there is not enough

information available to reach a decision. The weighted normalized decision matrix according to the following Equation 4.

$$w_{j=}\frac{1}{n} \tag{3}$$

Where, n = number of value in the samples

$$V_{ij} = n_{ij}w_j \mathrm{i} = 1, 2, \ldots \mathrm{m}, \mathrm{j} = 1, 2, \ldots \mathrm{n}. \tag{4}$$

Step 4: Determine the positive and negative ideal solution as follows:

$$Vp = \left\{V_1^+, V_2^+, \cdots, V_n^+\right\} = \left\{\left(max_i V_{ij}/j\mathcal{E}K\right), \left(min_i V_{ij}/j\mathcal{E}K'\right)/i = 1, 2, \cdots, m\right\} \tag{5}$$

$$Vn = \left\{V_1^-, V_2^-, \cdots, V_n^-\right\} = \left\{\left(min_i V_{ij}/j\mathcal{E}K\right), \left(max_i V_{ij}/j\mathcal{E}K'\right)/i = 1, 2, \cdots, m\right\} \tag{6}$$

Where, K = index set of the positive criteria

K' = index set of cost the negative criteria

Step 5: Determining distance as of the positive ideal solution (V_j^+)and negative ideal solution (V_j^-), and calculate the segregation using the 3D Euclidean distance n. The positive ideal solution shows the best possible performance for each criterion by taking the highest values across all alternatives. Conversely, the negative ideal solution represents the worst possible performance by taking the lowest values across all alternatives for each criterion. The positive and negative ideal solutions play crucial roles in determining the optimal choice among alternatives based on multiple criteria. The separation of each alternative provides the ideal solution and the ideal negative solution. The two Euclidean distance for each alternative are calculated as follows:

$$S_i^+ = \sqrt{\sum_{j=1}^{n}\left(V_{ij} - V_j^+\right)^2}\,\mathrm{j} = 1, 2, \cdots \mathrm{n}, \mathrm{i} = 1, 2, \cdots, \mathrm{m} \tag{7}$$

$$S_i^- = \sqrt{\sum_{j=1}^{n}\left(V_{ij} - V_j^-\right)^2}\,\mathrm{j} = 1, 2, \cdots \mathrm{n}, \mathrm{i} = 1, 2, \cdots, \mathrm{m} \tag{8}$$

Step 6: Find the relative closeness (C_i) to the ideal solution according to Equation 9. The C_i value closer to the positive ideal solution and farther from the negative ideal solution, thus ranking higher in preference.

$$C_i = \frac{S_i^-}{S_i^+ + S_i^-}, \mathrm{i} = 1, 2, \cdots \mathrm{m}; 0 \le C_i \le 1 \tag{9}$$

Step 7: Ranking of alternatives: rank the variable importance according to performance scores. The highest value of C_i is ranked as the most important variable, and the lowest value is ranked as the least important variable.

HVI test

The HVI tests were performed on the composites using a range of impact energies until the complete perforation of the composite, therefore the specific perforation energies were obtained from the composites considered in this research. The tests employed a sharp-nosed steel bullet measuring 8.5 mm in diameter, 13 mm in overall length, and weighing 5 g. The sharp-nosed steel bullet is chosen for its superior penetration capabilities and displays a pronounced phenomenon of local extrusion perforation (Q. Zhu et al. 2019), making it an optimal choice for evaluating the impact resistance of

materials. Specimens for the HVI tests were prepared in a square shape with sizes of 100 mm × 100 mm. Any debris or foreign materials adhering to the samples after impact testing were carefully removed. The plate samples were clamped onto a steel support and bolted into a steel block at each corner.

The tests were conducted using a gun tunnel system of 365 mm length and a bore of 20 mm in the Ballistic lab, Department of Aerospace Engineering, Universiti Putra Malaysia, Malaysia. A schematic illustration of the compressed gas gun set-up is shown in Figure 1. The helium gas which generated from the gas cylinder was sent to the pressurizing chamber. By adjusting the pressure control system settings, bullets were pressurized and accelerated horizontally through the gas gun tunnel into the impact chamber, achieving different impact velocities (V_i). A high-speed camera, capable of recording at 40,000 frames per second (fps) with an image size of 512 pixels per image (ppi), was positioned alongside the specimen and connected to a computer. This setup enabled precise measurement of the bullet's initial velocity (V_i) and the corresponding residual velocity (V_r). Figure 2 displays images of the test setup.

A considerable number of studies initiate HVI tests for FMLs and carbon fiber reinforced polymers at an approximate velocity of 70 m/s (Pernas-Sánchez et al. 2023; Sharma et al. 2021). Considering that this speed aligns with the equipment's minimum pressure setting of 2 bar (a velocity around 70 m/s), it was selected as the baseline for this experiment. Accordingly, six impact velocities of hybrid FMLs (2 bar, 3 bar, 4 bar, 5 bar, 7 bar, and 9 bar) were considered in ascending order for this study. The impact velocities of the bullet before and after penetration of the composites were recorded. The energy absorption of the hybrid FMLs was calculated using the Equation 10 (Stephen et al. 2022), which quantifies the energy absorbed by the FMLs as the difference between the initial kinetic energy of the projectile and its residual kinetic energy after passing through the FMLs. For better understanding of the impact response of the FMLs composites, the specific energy absorption (SEA) was calculated using the Equation 11 (Boursier, Ciardiello, and Tridello 2022). SEA provides information on the absorbing capability efficiency and is crucial to the development of components that require weight reduction, such as in automotive or aerospace applications (Esnaola et al. 2016).

$$E_a = \frac{1}{2} m\left(V_i^2 - V_r^2\right), \tag{10}$$

Where E_a = energy absorption by materials (J),
m = mass of projectile (kg).
The SEA was obtained from Equation 11:

$$E_a = \frac{E_a}{M} \tag{11}$$

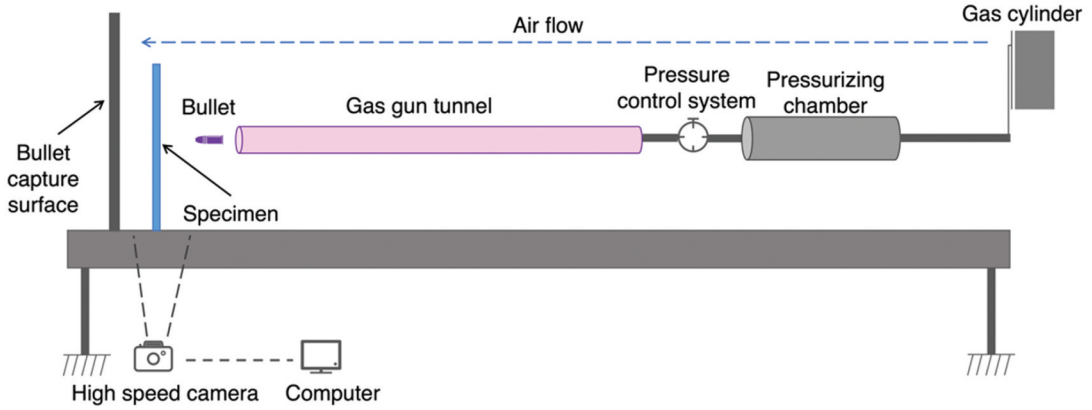

Figure 1. Schematic illustration of compressed air gun set up used for HVI test.

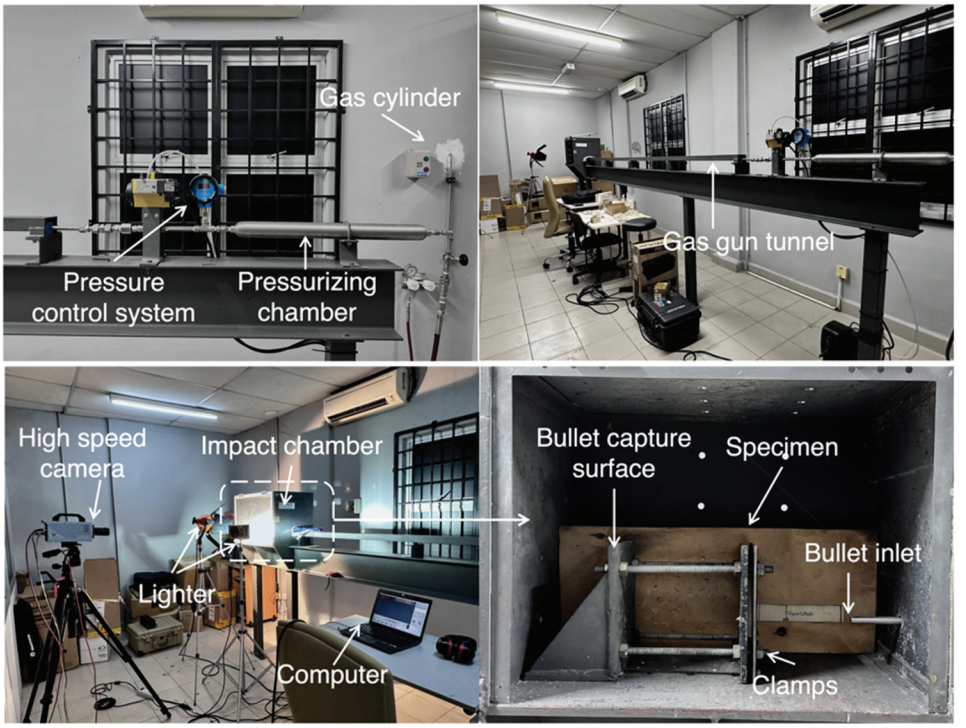

Figure 2. Experiment HVI test facility set-up.

Where E_a = energy absorption by materials (J),
M = mass of the plate (g)

NDT test

To accurately assess the damage mechanisms of FMLs ACPCA following HVI testing, it is essential to employ complementary detection methods. In this study, we combined IR and RT to examine the damage inflicted upon hybrid FMLs ACPCA under various HVI conditions. After HVI testing, IR is employed to scan the material's surface and detect different thermal signatures in areas with internal damage compared to undamaged regions (J. Zhu et al. 2022). RT provides real-time, high-resolution imaging that enables precise measurement and evaluation of damage, offering critical information for assessing the structural integrity of the material (Nsengiyumva et al. 2021). For IR testing, temperature variations on the specimen surface were monitored using an infrared camera, specifically, the OPTRIS PI 640i (Germany), operating at a frame rate of 60 hz. Heat lamps (max power 500 W) as external stimulus sources were employed, providing adequate thermal contrasts. The heat lamps were positioned 40 cm from the specimen, and the infrared camera was stationed at a fixed distance of 100 cm from the specimen. RT involved the use of X-rays, which penetrated the test piece to identify defects. RT was employed for image processing, utilizing a Digital Detector Array operating at 80 kV. The source-to-detector system was configured at a distance of 700 mm. All the specimens were analyzed from both impact and bottom sides. The OPTRIS PI software was employed to capture IR images, while the ISee software facilitated the analysis of the RT images.

SEM test

SEM plays a crucial role in examining the surface topography of materials, providing detailed insights into damage mechanisms and structural integrity. The SEM was employed to examine the surface topography of the FMLs after HVI test, providing a detailed analysis of damage mechanisms induced by the impact. The samples for SEM analysis were prepared by cutting the impacted FMLs into small sections measuring 1 mm × 1 mm. These samples were then meticulously prepared for SEM examination. To enhance the resolution and contrast of the SEM images, the cross-section and fractured surfaces of the FMLs were sputter-coated with a thin layer of gold prior to each analysis. The SEM analysis was performed using a JEOL JSM-6400 scanning electron microscope.

Results and discussions

TOPSIS results

In order to balance the weight and mechanical properties of FMLs for potential automotive applications, the TOPSIS method was utilized to select the optimal laminate among four FMLs. In this research, the decision-making criteria are obtained from the tensile, flexural, ILSS, Izod impact strengths, hardness, and density of the FMLs. A decision matrix detailing these properties is presented in Table 1 (Jha et al. 2022). From Table 1, we can conclude that the specimen ACPCA exhibits the best mechanical performance among other layer sequences of FMLs. Specifically, ACPCA shows the highest tensile strength (408.44 MPa), which is crucial for resistance to elongation. Additionally, ACPCA also exhibits the highest flexural strength (360.54 MPa), indicating superior resistance to bending. The interlaminar shear strength is highest in ACPCA (24.04 MPa), suggesting better bonding between layers. Moreover, ACPCA demonstrates the highest impact strength (171.43 kJ/m^2), indicating superior impact resistance. ACPCA also shows the highest hardness (25.99 hR), indicative of better surface resistance. However, from a weight saving perspective, CPAPC has the lowest density (1.36 g/cm^3), which is advantageous for weight reduction in automotive applications.

All the elements are normalized by Equation 2, with the normalized values facilitating comparison by standardizing all criteria onto a common scale. The normalization matrix is presented in Table 2, where ACPCA consistently exhibits the highest normalized values across most criteria, emphasizing its overall superiority. Table 3 shows the normalized weighted decision matrix, which incorporates

Table 1. Decision matrix of hybrid FMLs.

FMLs	Tensile strength (MPa)	Flexural strength (MPa)	ILSS (MPa)	Izod impact strength (kJ/m^2)	Hardness (HR)	Density (g/cm^3)
APPPA	115.78	136.01	12.89	107.42	19.50	1.48
standard deviation	3.68	8.03	0.73	6.14	1.18	0.06
APCPA	246.77	229.22	19.04	123.88	22.50	1.66
standard deviation	10.13	14.79	0.63	10.01	1.34	0.06
ACPCA	408.44	360.54	24.04	171.43	25.99	1.80
standard deviation	12.97	43.04	0.03	20.48	1.71	0.05
CPAPC	294.16	156.33	13.1	97.77	24.26	1.36
standard deviation	9.61	29.49	1.01	0.17	0.81	0.02

Table 2. Normalized decision matrix.

FMLs	Tensile strength (MPa)	Flexural strength (MPa)	ILSS (MPa)	Izod impact strength (kJ/m^2)	Hardness (HR)	Density (g/cm^3)
APPPA	0.169	0.200	0.198	0.198	0.197	0.384
APCPA	0.360	0.337	0.292	0.229	0.227	0.431
ACPCA	0.596	0.530	0.369	0.316	0.262	0.467
CPAPC	0.429	0.230	0.201	0.180	0.245	0.353

Table 3. Normalized weighted matrix.

FMLs	Tensile strength (MPa)	Flexural strength (MPa)	ILSS (MPa)	Izod impact strength (kJ/m^2)	Hardness (HR)	Density (g/cm^3)
APPPA	0.028	0.033	0.033	0.033	0.033	0.064
APCPA	0.060	0.056	0.049	0.038	0.038	0.072
ACPCA	0.099	0.088	0.061	0.053	0.044	0.078
CPAPC	0.072	0.038	0.034	0.030	0.041	0.059

Table 4. Positive and negative ideal solution.

FMLs	Tensile strength (MPa)	Flexural strength (MPa)	ILSS (MPa)	Izod impact strength (kJ/m^2)	Hardness (HR)	Density (g/cm^3)
Ideal solution	0.099	0.088	0.061	0.053	0.044	0.059
Negative solution	0.028	0.033	0.033	0.033	0.033	0.078

Table 5. Euclidean distance as of ideal solution or the lowest point solution.

FMLs	S_i^+	S_i^-
APPPA	0.097	0.014
APCPA	0.056	0.044
ACPCA	0.019	0.097
CPAPC	0.067	0.049

criteria weights determined using the mean value method (Ardil 2021). Subsequently, the positive and negative ideal solutions were identified and summarized in Table 4. According to the results from positive and negative ideal solution, the two Euclidean distance for each alternative are calculated as shown in Table 5. The Euclidean distance results indicated that the ACPCA is closest to the ideal solution and farthest from the negative solution, validating its selection as the optimal configuration. Finally, the relative closeness (C_i) values were calculated , and the ranks of alternatives are summarized in Table 6. The ranking order is ACPCA – APCPA – CPAPC – APPPA, suggesting that the hybrid FMLs ACPAC are the most preferred FMLs with the maximum value of C_i based on the six criteria evaluated, while A/P/P/P/A ranks last with the lowest value (0.126), indicating it is the least preferred.

From TOPSIS results, despite having a slightly higher density, ACPCA offers a balanced profile of weight and mechanical properties, which is critical for automotive components where performance cannot be compromised. While CPAPC offers a lower density advantageous for weight reduction, it does not surpass ACPCA in mechanical properties. Thus, the CPAPC may be suitable for applications prioritizing weight reduction over mechanical strength. APCPA strikes a balance but falls short compared to ACPCA. APPPA exhibits lower mechanical values affecting its rank, despite a decent density. The high rankings of ACPCA underscore the importance of tensile strength, flexural strength, and impact resistance in automotive applications, where mechanical robustness is paramount. Therefore, for applications requiring robust mechanical strength and impact resistance, ACPCA emerges as the preferred choice. In conclusion, the TOPSIS method has effectively highlighted ACPCA as the superior FMLs for automotive applications due to its high performance across all key

Table 6. The rank and the relative closeness (C_i^-) to the ideal solution.

FMLs	C_i^-	Rank
APPPA	0.126	4
APCPA	0.440	2
ACPCA	0.836	1
CPAPC	0.422	3

mechanical criteria, despite having a slightly higher density. Looking ahead, ACPCA sets a benchmark, motivating future designs to match or exceed its properties while exploring avenues to reduce density.

High velocity impact test results

The experimental HVI test results are presented in Table 7, and the post-impact images captured by the high-speed camera during these tests are presented in Figure 3. From the results, the ACPCA specimen is considered to have absorbed all the impact energy under 4 bar. Specifically, the hybrid ACPCA specimen effectively stopped the sharp-nosed steel bullet by use of 2 bar (73.33 m/s) and 3 bar (86.08 m/s), where the bullet totally rebounded after impact. At 4 bar (92.33 m/s), the specimen halted the bullet without complete perforation. However, it can be seen in the post-impact video that the bullet rebounds slowly post-impact, following a gradual parabolic descent at 92.33 m/s. The findings indicate that this velocity of bullet approaches the ballistic limit of specimen ACPCA. The ballistic limit is defined as the highest impact velocity at which a bullet does not penetrate the specimen. Additionally, from Table 7, it is evident that the Ea value increased as the impact velocity increased before sample penetration, and the SEA value also increased from 34.64% to 54.81%.

Under the higher impact velocity (101.35 m/s, 132.96 m/s, and 144.27 m/s), all specimens were completely penetrated during impact, resulting in impact debris and left behind a hole at the impact zone. At 101.35 m/s, the energy absorbed by ACPCA is nearly the same as that under an impact velocity of 92.33 m/s. These results further confirm that the ballistic limit falls within the 92.33 m/s to 101.35 m/s range. Previous research indicates that the ballistic limit of CF-reinforced Al laminates (CRALLs 2/1) is approximately 70 m/s (Q. Zhu et al. 2019). The integration of PALF in hybrid FMLs ACPCA demonstrates a notable improvement in ballistic performance. In this velocity range, the Ea values ranged from approximately 21.31 J to 21.82 J, while the SEA was between 54.81% and 56.12%. The maximum Ea values (29.74 J) and SEA (76.49%) were achieved at 132.96 m/s. Interestingly, these

Table 7. Experimental HVI test results.

Specimen ACPCA	Pressure (bar)	V_i (m/s)	V_r (m/s)	E_a (J)	SEA(%)
	2	73.33	-	13.44	34.64
	3	86.08	-	18.52	47.63
	4	92.33	-	21.31	54.81
	5	101.35	39.31	21.82	56.12
	7	132.96	76.03	29.74	76.49
	9	144.27	98.83	27.62	71.04

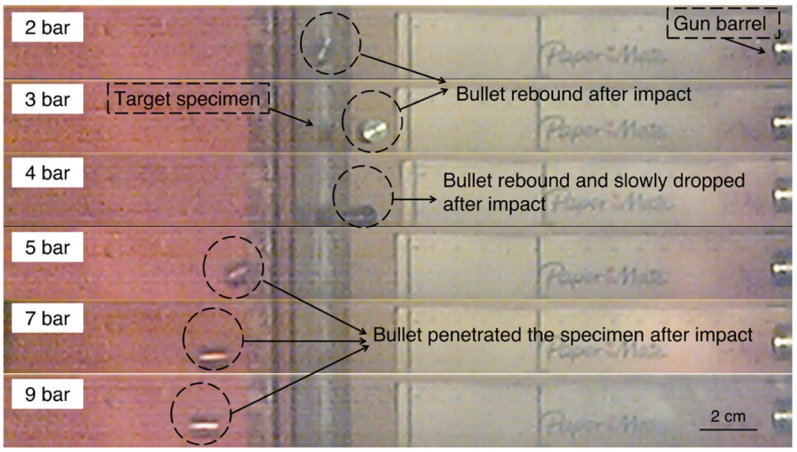

Figure 3. Hybrid ACPCA laminates post-impact caught on high speed camera.

values surpass those observed at 144.27 m/s, indicating that an impact velocity of 132.96 m/s is more than adequate for the hybrid FMLs ACPCA.

Visual inspection

The visual inspection of hybrid FMLs under different impact energies is presented in Figure 4 and 5. In Figure 4, the hybrid FMLs ACPCA exhibited only surface cracking on the impact face and no penetration under an impact velocity of 73.33 m/s, which means the ACPCA can withstand some extent of impact force. As the impact velocity increased to 86.08 m/s, cracks appeared in ACPCA composites on both the impact and bottom face, although the specimen remained unpenetrated by the bullet. However, despite not being fully penetrated, the specimen nearly succumbed with an impact velocity of 92.33 m/s, resulting in a small hole on the impact face, and an open crack emerged on the bottom face, further indicating the substantial impact effects. When the impact velocities exceeding 92.33 m/s (101.35 m/s, 132.96 m/s, and 144.27 m/s), the ACPCA specimens were totally penetrated, resulting in a visible throughout hole in the specimens. Figure 4b reveals that at impact velocity of 101.35 m/s and 132.96 m/s, triangular bullet imprints were left on the bottom face of the samples. However, at 144.27 m/s, the imprint resembled that of a sharp-nosed steel bullet with four corners, suggesting that the sample's ability to replicate the bullet's shape intensifies with increasing impact velocity.

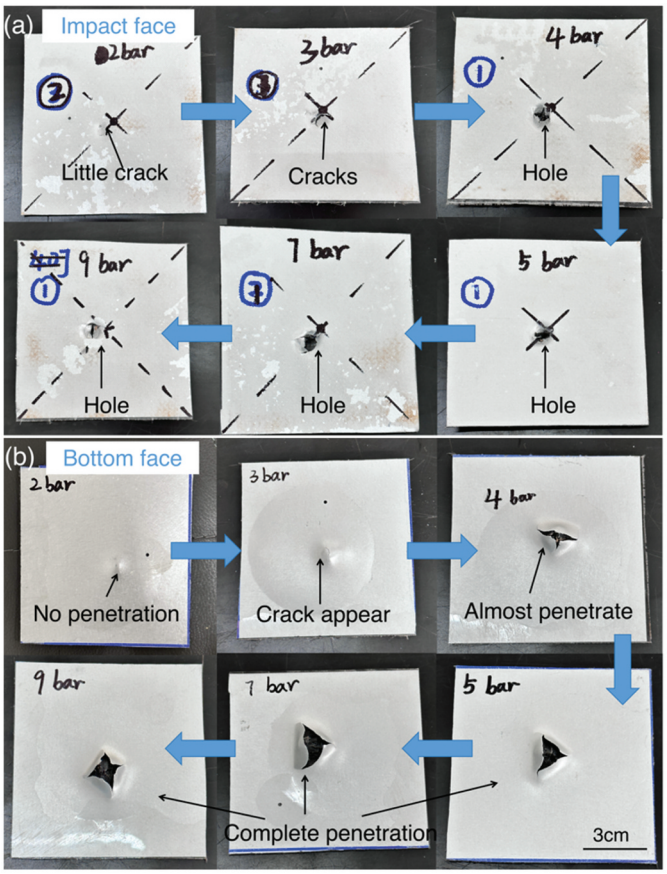

Figure 4. Post-impact images of specimen subjected to experimental HVI tests with different impact velocity (face and bottom): (a) impact face (b) bottom face.

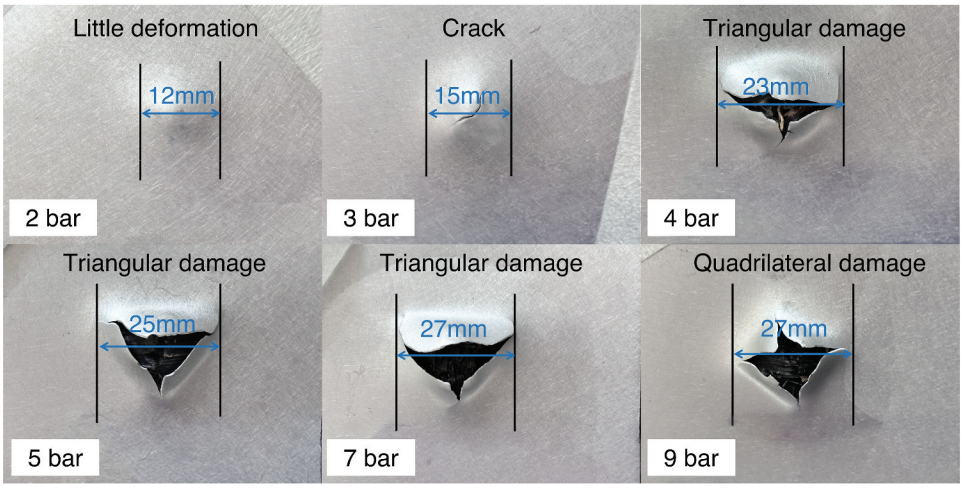

Figure 5. The damage shape and size of hybrid FMLs subjected to different impact velocity.

As illustrated in Figure 5, an increase in impact energy from 73.33 m/s to 144.27 m/s resulted in a 125% expansion in the damage diameter of the ACPCA, suggesting an enhanced energy absorption capacity of the hybrid FMLs. When subjected to impact velocity of 101.35 m/s and 132.96 m/s, the fracture range of the penetrated samples extended from 25 mm to 27 mm. This suggests that greater plastic deformation of the aluminum layers contributes to increased energy absorption by the sample. Upon further observation of the samples subjected to impact velocity of 132.96 m/s and 144.27 m/s, it was noted that even though the bullet replication varied, the extent of damage remained steady at 27 mm. Cross-referencing this with the data from the HVI tests (Table 7) revealed a surprising similarity in the energy absorbed by the samples at both impact energy levels. This observation supports the idea that the energy absorption capacity of FMLs is closely linked to the extent of aluminum deformation upon complete penetration. Shayan et al. (Shahjouei, Barati, and Tooski 2021) also pointed out that combining aluminum alloy sheets with suitable epoxy results in composites with enhanced energy absorption, high strength, and an excellent stiffness-to-weight ratio under impact loads. This is further supported by Mohammadi et al. (Mohammadi et al. 2023), which highlights that metallic sandwich structures dissipate energy through plastic deformation, effectively absorbing impact energy during automotive collisions.

NDT results

IR test results

The images obtained from the IR tests are shown in Figures 6 and 7. As illustrated in Figure 6, because of the equipment limitations, no damage was captured in the ACPCA composites on either the impact face or bottom face when subjected to an impact velocity of 73.33 m/s. This suggests that the hybrid FMLs ACPCA can absorb the impact force at lower impact velocity ranges where damage is not detectable in IR images. At an impact velocity of 86.08 m/s, there is still no notable damage appeared on the impact face of the ACPCA. However, a circular bright area appears on the bottom face in the IR images. These findings are consistent with the visual inspection as shown in Figure 4. A crack appears on the bottom face under the 3 bar pressure (86.08 m/s), while no crack is visible on the bottom face under the 2 bar pressure (73.33 m/s). When the ACPCA composites were subjected to an impact velocity of 92.33 m/s, a clear circular shape appears on both the impact face and the bottom face, surrounded by a circular shadow. These results suggest that an impact velocity of 92.33 m/s leads to

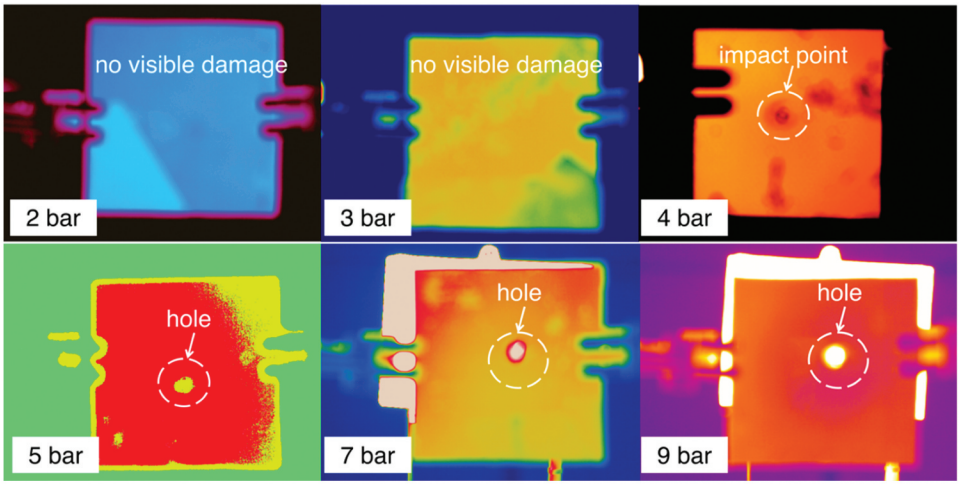

Figure 6. IR impact face results of hybrid FMLs ACPCA after high-velocity impact.

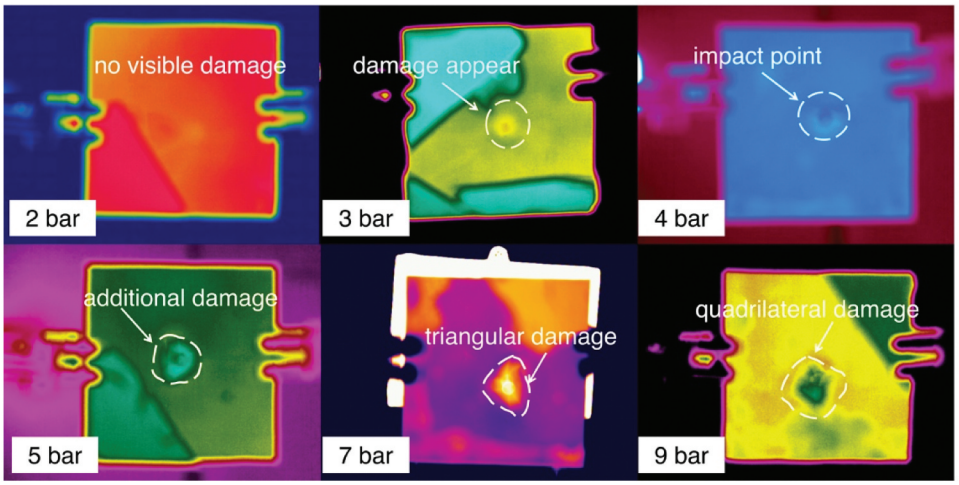

Figure 7. IR bottom face results of hybrid FMLs ACPCA after high-velocity impact.

significant damage in the ACPCA composites. This could be due to the increased energy causing more severe deformation and damage.

When the impact velocity is increased further to 101.35 m/s, 132.96 m/s, and 144.27 m/s, a bright damaged area becomes visible in the IR images of the impact face (as shown in Figure 6). This suggests that the bullet has penetrated through the specimen, creating a hole. This observation is consistent with the visual findings presented in Figure 4. The increased impact energy leads to more severe damage, including complete perforation, further demonstrating the effects of high-energy impacts on the integrity of the ACPCA composites. Figure 7 presents the damage on the bottom face of the ACPCA material at a velocity of 101.35 m/s, 132.96 m/s, and 144.27 m/s. From Figure 7, the color is fading toward the impact point, suggesting that the material has sustained additional damage types around this area, such as internal damage, deformation, and delamination. This results also largely align with the visual observations in Figure 4. Interestingly, these irregular and contrasting damage marks are primarily concentrated near the impact point. This damage pattern is consistent with the principles of HVI, which differ from those of LVI. In LVI scenarios, the damage tends to be more

extensive around the impact area. In contrast, for specimens subjected to HVI, the damage is localized at the point of impact. The shock waves produced during the HVI of a bullet on the target specimen do not propagate to areas far from the impact location due to the minimal interaction time between the bullet and the specimen, resulting in localized impact damage. These findings align with previous research (Stephen et al. 2022). However, further details, such as the shape of the fracture hole, need to be further confirmed with RT results.

RT results

The RT test results reveal consistent damage patterns on both the impact face (Figure 8) and the bottom face (Figure 9) of ACPCA composites across varying impact energies. As shown in Figures 8 and 9, more significant damage is induced in ACPCA by higher impact energies. At an impact velocity

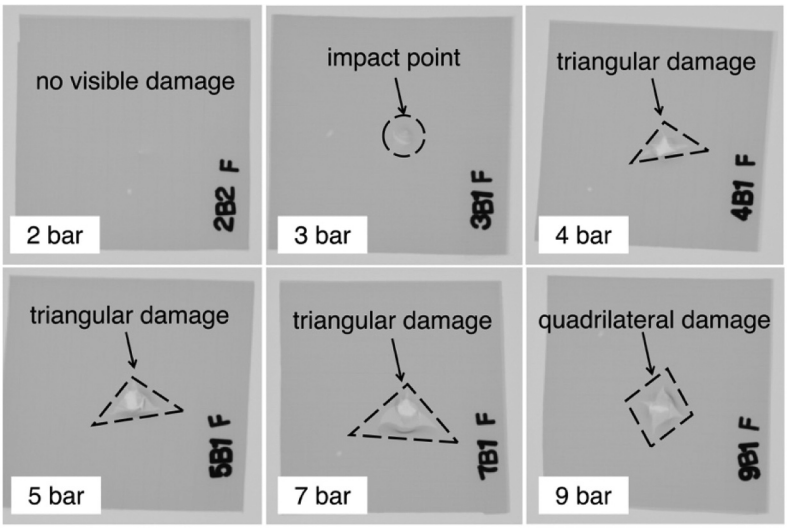

Figure 8. RT impact face results of hybrid FMLs ACPCA after high-velocity impact.

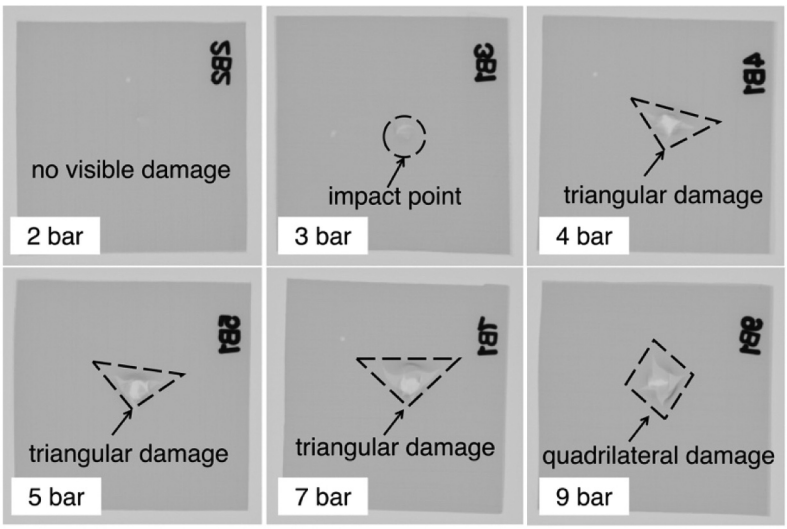

Figure 9. RT bottom face results of hybrid FMLs ACPCA after high-velocity impact.

73.33 m/s, the RT results showed a light point at the center of the specimen, which corresponds to the impact point. However, no cracks were observed at this energy level. This finding is in line with the visual inspection results presented in Figure 4. When the impact velocity was increased to 86.08 m/s, although no hole was observed at the center of the specimen, a significant crack appeared, indicating concentrated damage at the impact point. This suggests that the material is beginning to fail under this increased energy, even though complete penetration has not yet occurred. When the impact velocity was increased beyond 86.08 m/s (to 92.33 m/s, 101.35 m/s, 132.96 m/s, and 144.27 m/s), holes were observed at the center of all the specimens. Among these, the specimen subjected to 4 bar (92.33 m/s) showed a significantly smaller damage area than the others, despite also having a hole at the center. This observation aligns with the results from the HVI testing, where the bullet was seen to rebound slowly following impact, tracing a gradual parabolic descent at a velocity of 92.33 m/s in the post-impact video. This suggests that the speed of the bullet at an impact velocity of 92.33 m/s during the HVI is approximately equal to the penetration speed of the ACPCA specimen.

At higher velocities (101.35 m/s, 132.96 m/s, and 144.27 m/s), additional damage around the impact area is evident, forming a light-gray ring around the impact point. This suggests significant surrounding damage due to stress wave propagation. Among these varying impact energies, the largest damage area was observed at a velocity of 132.96 m/s. This outcome is consistent with the HVI testing results, where the maximum Ea values of 29.74 J and SEA of 76.49% were achieved at a velocity of 132.96 m/s. These findings indicate that a velocity of 132.96 m/s is more than sufficient to cause significant damage to the hybrid FMLs ACPCA. It's also noteworthy that, compared with IR testing, it can be observed that the macro-crack and damage shape were observed in all radiographic images and are much clearer than the IR images. The variation in the shape of damage or holes post HVI testing could be attributed to a multitude of potential factors. These may encompass changes in the impact angle during the acceleration of the bullet, differences in impact energy, bullet shapes, and the propagation of stress waves, among others (Q. Zhu et al. 2019). These aspects require further comprehensive investigation to fully understand their implications.

Damage mechanisms analysis

In order to investigate damage mechanisms in hybrid FMLs subjected to HVI loading, the cross-sections of failed specimens were subjected to SEM analysis. Figure 10 presents the different damage mechanisms observed in failed hybrid FMLs. The damage mechanisms occurred for the metal layers were metal plastic deformation, rupture, and delamination. After HVI testing, all studied FMLs were found to experience delamination because of the insufficient adhesion between the FRP and the Al layers. Thus, the SEM analysis only focus on the FRP composite layers because the Al layer was already detached with FRP layers after band saw cutting. As discerned through SEM, the damage mechanisms observed for the FPR composites were fiber breakage, fiber pull out, matrix cracking, and composite delamination. In addition, combining the IR and RT images (Figures 6–9) with the SEM results (Figure 10) reveals that with the increase in impact velocity, the phenomena of delamination, fiber breakage, and fiber pulling out increase, making the damage to the material becomes more obvious.

According to a previous research (Stephen et al. 2022), delamination usually happens in the early phase of impact when the bullet contacts the laminates. This is attributed to the difference in bending stiffness between various reinforcements and the matrix. Therefore, in Figure 10c, we can identify the delamination that occurs between the CF layer and the PALF layer. The delamination helps dissipate impact energy under HVI, but excessive delamination will increase susceptibility to additional damage and reduce energy absorption efficiency. The debonding of the CF is clearly visible in Figure 10b. Additional damage, particularly matrix cracking in Figure 10d, results from shear loading in the transverse direction. Fiber breakage occurs due to localized stress concentrations from HVI, fracturing fibers near impact sites and spreading outward. As the impact progresses, fiber breakage occurs due to high bending stress, which results in a loss of residual tensile strength in the FRP layers. This weakening reduces the composite's load-bearing capacity and overall efficiency in absorbing energy.

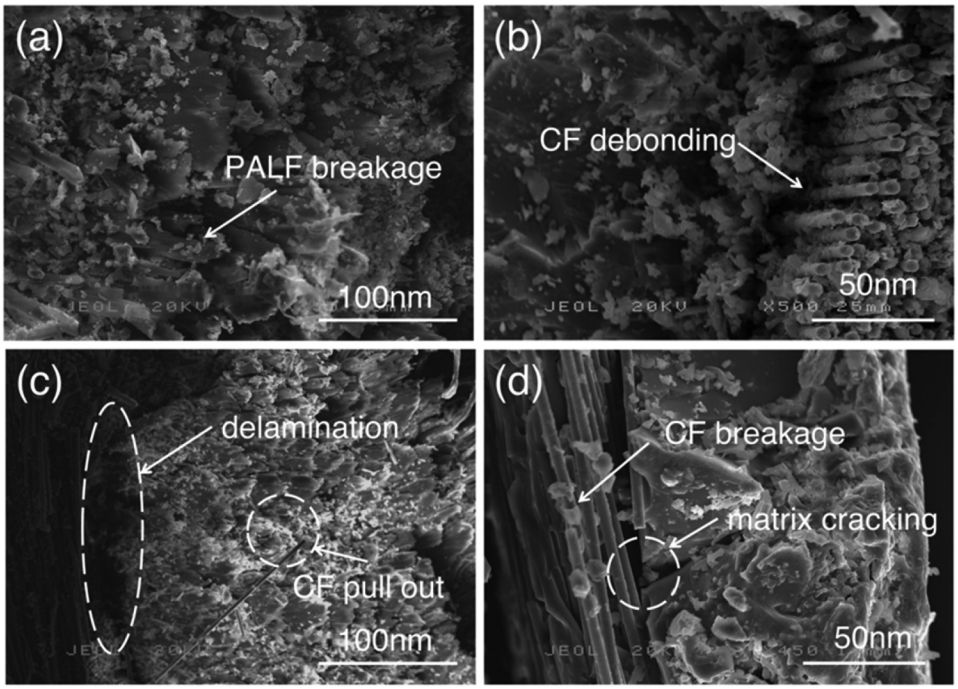

Figure 10. SEM images of different damage mechanisms of hybrid FMLs ACPCA after HVI test.

In Figure 10a, the PALF layer exhibits a completely brittle broken surface due to its inferior tensile performance. However, in Figure 10d, the high tensile strength and modulus of the unidirectional CF result in incomplete CF layer breakage following matrix cracking. Therefore, in the selected FMLs (ACPCA), with CF on the outside and PALF on the inside, demonstrate excellent HVI resistance, leveraging the superior impact resistance of CF to enhance overall structural integrity and energy absorption. These results are consistent with previous studies (H. Y. Xiao et al. 2024), which demonstrated significant improvements in Izod impact strength. Specifically, ACPCA showed a 59.59% improvement in Izod impact strength compared to non-hybrid FMLs APPPA and a 38.38% increase compared to APCPA, which incorporates only one layer of CF. These findings suggest that ACPCA is particularly suitable for applications requiring high impact resistance in the automotive industries such as door panels, bumpers, etc.

Conclusion

This research employed TOPSIS method to select an optimal hybrid FMLs ACPCA and manufactured the selected FMLs using the VARTM process. The HVI test was performed on the composites for a range of impact energies until the composites were completely perforated. Through visual inspection, IR, RT, and SEM methods, a comprehensive understanding of the material's response to different impact energies was achieved. The experimental results demonstrated that the initial penetration velocity falls within the 92.33 m/s to 101.35 m/s range, where the ACPCA specimen stopped all the bullets at a velocity of 92.33 m/s without undergoing complete perforation. Full penetration occurred at a higher impact velocity (101.35 m/s, 132.96 m/s, and 144.27 m/s), with the maximum energy absorption values (29.74 J) and SEA (76.49%) achieved at an impact velocity of 132.96 m/s. Visual inspections, IR, and RT consistently illustrated the damage progression under varying impact energies, which almost align with the HVI results. More significant damage was induced on ACPCA by higher impact energies, and the damage

diameter expanded by 125% as the impact velocity increased from 73.33 m/s to 144.27 m/s. At higher impact velocity of 101.35 m/s, 132.96 m/s, and 144.27 m/s, additional damage around the impact point was clearly visible. The IR and RT results indicate additional damage around the impact point, corroborated by SEM evidence of matrix cracking, delamination, fiber breakage, and fiber pull-out during HVI testing.

In conclusion, this study provides valuable insights into the impact behavior and damage mechanisms of hybrid FMLs under HVI loading. This thorough investigation provides a more complete understanding of the material's response to different impact energies, which is crucial for automotive safety applications. The thorough investigation of FMLs ACPCA offers a well-balanced combination of lightness, environmental friendliness, and mechanical performance, making it particularly beneficial for automotive safety applications. These FMLs can be effectively incorporated into vehicle designs, such as door panels, roof structures, and bumpers, to enhance passenger safety during high-speed collisions. Given that such impacts are a common challenge in the automotive industry, our research holds significant relevance and potential for real-world application.

Acknowledgments

The authors would like to thank the Department of Aerospace Engineering, Faculty of Engineering, Universiti Putra Malaysia, Laboratory of Biocomposite Technology, Institute of Tropical Forestry and Forest Product (INTROP), Universiti Putra Malaysia, and Industrial Technology Division, Malaysian Nuclear Agency, for the close collaboration in this research.

Disclosure statement

No potential conflict of interest was reported by the author(s).

Funding

The authors would like to thank Universiti Putra Malaysia for the financial support through Geran Inisiatif Putra Siswazah (GP-IPS) with grant number 9739200.

ORCID

Mohamed Thariq Hameed Sultan http://orcid.org/0000-0002-5110-0242

Author contributions

Conceptualization, HX; methodology, HX; formal analysis, HX; investigation, HX, MIN, SMMA; resources, MTHS; data curation, HX; writing – original draft preparation, HX; writing – review and editing, MTHS, FSS, SYN, MIN, SMMA, and SR; visualization, HX; supervision, MTHS and SYN; project administration, FSS, and SYN; funding acquisition, MTHS, and SYN. All authors have read and agreed to the published version of the manuscript.

Data availability statement

The authors confirm that the data supporting the findings of this study are available within the article.

Highlights

(1) By using Technique for Order Preference by Similarity to the Ideal Solution (TOPSIS) method, the best-performing hybrid fiber-metal laminates (FMLs), ACPCA, were identified from four layer sequences (APPPA, ACPCA, APCPA, and CAPAC), and then fabricated by vacuum assist resin tranfer molding (VARTM).

(2) The high-velocity impact (HVI) behavior of FMLs was observed under a range of impact velocities (73.33 m/s, 86.08 m/s, 92.33 m/s, 101.35 m/s, 132.96 m/s, and 144.27 m/s), and the damage modes and failure were characterized combining visual inspection, infrared thermography (IR), radiography testing (RT), and scanning electron microscopy (SEM).
(3) The results highlight that the hybrid FMLs (ACPCA) with satisfied energy absorption ability are well suited for applications in the automotive industries, especially parts that need to balance impact resistance and lightweight performance.

References

Abdel-Basset, M., A. Gamal, M. Elhoseny, and M. A. Hossain. 2024. "Chapter 2 - an Eclectic Decision for Selecting the Optimum Green Energy Source for Sustainable Energy Planning by Considering Multifactors." In *Multi-Criteria Decision-Making for Renewable Energy*, edited by P. Edward, 7–36. 1st ed. Amsterdam: Elsevier.

Ahmadijokani, F., A. Shojaei, S. Dordanihaghighi, E. Jafarpour, S. Mohammadi, and M. Arjmand. 2020. "Effects of Hybrid Carbon-Aramid Fiber on Performance of Non-Asbestos Organic Brake Friction Composites." *Wear* 452-453:203280–203453. https://doi.org/10.1016/j.wear.2020.203280.

Almomani, M. A., Q. M. Mahafdeh, A. Almomani, and O. Bataineh. 2024. "Correction: Selecting the Best Thermal Barrier Coating Material for Hot Sections in Gas Turbine Using AHP and TOPSIS Multi-Criteria Decision Making Techniques." *International Journal on Interactive Design & Manufacturing (IjideM)* 18 (6): 4187–4187. https://doi.org/10.1007/s12008-024-02004-9.

Andrew, J. J., S. M. Srinivasan, A. Arockiarajan, and H. N. Dhakal. 2019. "Parameters Influencing the Impact Response of Fiber-Reinforced Polymer Matrix Composite Materials: A Critical Review." *Composite Structures* 224:111007. https://doi.org/10.1016/j.compstruct.2019.111007.

Ardil, C. 2021. "Freighter Aircraft Selection Using Entropic Programming for Multiple Criteria Decision Making Analysis." *International Journal of Computer Mathematics* 15:119–126. https://orcid.org/0000-0003-2457-7261 .

Arredondo-Galeana, A., B. Yeter, F. Abad, S. Ordóñez-Sánchez, S. Lotfian, and F. Brennan. 2023. "Material Selection Framework for Lift-Based Wave Energy Converters Using Fuzzy TOPSIS." *Energies (Basel)* 16 (21): 7324. https://doi.org/10.3390/en16217324.

Bisheh, H. 2024. "Design and Analysis of Hybrid Natural/Synthetic Fibre-Reinforced Composite Automotive Drive Shafts." *Structures* 61:106057. https://doi.org/10.1016/j.istruc.2024.106057.

Boursier, N. C., R. Ciardiello, and A. Tridello. 2022. "Experimental and Numerical Investigation of a Lattice Structure for Energy Absorption: Application to the Design of an Automotive Crash Absorber." *Polymers* 14 (6): 1116. https://doi.org/10.3390/polym14061116.

Chee, S. S., M. Jawaid, M. T. H. Sultan, O. Y. Alothman, and L. C. Abdullah. 2019. "Accelerated Weathering and Soil Burial Effects on Colour, Biodegradability and Thermal Properties of Bamboo/Kenaf/Epoxy Hybrid Composites." *Polymer Testing* 79:106054. https://doi.org/10.1016/j.polymertesting.2019.106054.

Chiachío, M., J. Chiachío, A. Saxena, and K. Goebel. 2016. "16 - an Energy-Based Prognostic Framework to Predict Evolution of Damage in Composite Materials." In *Structural Health Monitoring (SHM) in Aerospace Structures*, edited by F. Yuan, 447–477. Woodhead, Cambridge: Woodhead Publishing.

Dadej, K., and J. Bieniaś. 2020. "On Fatigue Stress-Cycle Curves of Carbon, Glass and Hybrid Carbon/glass-Reinforced Fibre Metal Laminates." *International Journal of Fatigue* 140:105843. https://doi.org/10.1016/j.ijfatigue.2020.105843 .

Ding, Z., H. Wang, J. Luo, and N. Li. 2021. "A Review on Forming Technologies of Fibre Metal Laminates." *International Journal of Lightweight Materials and Manufacture* 4 (1): 110–126. https://doi.org/10.1016/j.ijlmm.2020.06.006.

Esnaola, A., I. Tena, J. Aurrekoetxea, I. Gallego, and I. Ulacia. 2016. "Effect of Fibre Volume Fraction on Energy Absorption Capabilities of E-Glass/polyester Automotive Crash Structures." *Composites Part B Engineering* 85:1–7. https://doi.org/10.1016/j.compositesb.2015.09.007.

Gardner, C., Y. Ko, M. Koutoumbas, E. Flynn, I. Cummings, and P. Cornwell. 2022. "Delamination Detection in Fiber Metal Laminates Using Ultrasonic Wavefield Imaging." *Rotating Machinery, Optical Methods & Scanning LDV Methods* 6:59–72. https://doi.org/10.1007/978-3-030-76335-0_6.

Germano, B. G., R. F. Assunção, J. César dos Santos, G. G. Pino, T. H. Panzera, and F. Scarpa. 2023. "Fully Biobased Composite and Fiber-Metal Laminates Reinforced with Cynodon Spp. Fibers." *Polymer Composites* 44 (1): 453–464. https://doi.org/10.1002/pc.27109.

Jha, M. K., S. Gupta, V. Chaudhary, and P. Gupta. 2022. "Material Selection for Biomedical Application in Additive Manufacturing Using TOPSIS Approach." *Materials Today: Proceedings* 62:1452–1457. https://doi.org/10.1016/j.matpr.2022.01.423.

Khalid, M. Y., A. Rashid, Z. U. Arif, M. F. Sheikh, H. Arshad, and M. A. Nasir. 2021. "Tensile Strength Evaluation of Glass/Jute Fibers Reinforced Composites: An Experimental and Numerical Approach." *Results in Engineering* 10:100232. https://doi.org/10.1016/j.rineng.2021.100232.

Khalid, M. Y., A. A. Rashid, and M. F. Sheikh. 2021. "Effect of Anodizing Process on Inter Laminar Shear Strength of GLARE Composite Through T-Peel Test: Experimental and Numerical Approach." *Experimental Techniques* 45 (2): 227–235. https://doi.org/10.1007/s40799-020-00433-1.

Khan, S. H., and A. P. Sharma. 2022. "Influence of Metal/Composite Interface on the Damage Behavior and Energy Absorption Mechanisms of FMLs Against Projectile Impact." *Defence Technology* 18 (3): 441–456. https://doi.org/10.1016/j.dt.2020.11.012.

Lawrence, S. B., D. Oguamanam, and H. Bougherara. 2022. "Impact Response of a New Kevlar/Flax/Epoxy Hybrid Composite Using Infrared Thermography and High-Speed Imaging." *Composite Structures* 280:114885. https://doi.org/10.1016/j.compstruct.2021.114885.

Liu, C., Y. X. Zhang, and L. Ye. 2017. "High Velocity Impact Responses of Sandwich Panels with Metal Fibre Laminate Skins and Aluminium Foam Core." *International Journal of Impact Engineering* 100:139–153. https://doi.org/10.1016/j.ijimpeng.2016.09.004.

Mattsson, K., L. A. Hansson, and T. Cedervall. 2015. "Nano-Plastics in the Aquatic Environment." *Environmental Science Processes & Impacts* 17 (10): 1712–1721. https://doi.org/10.1039/C5EM00227C.

Mohammadi, H., Z. Ahmad, M. Petrů, S. A. Mazlan, M. A. F. Johari, H. Hatami, and S. S. R. Koloor. 2023. "An Insight from Nature: Honeycomb Pattern in Advanced Structural Design for Impact Energy Absorption." *Journal of Materials Research and Technology* 22:2862–2887. https://doi.org/10.1016/j.jmrt.2022.12.063.

Monetto, I. 2019. "The Effects of an Interlayer Debond on the Flexural Behavior of Three-Layer Beams." *Coatings* 9 (4): 258. https://doi.org/10.3390/coatings9040258.

Murugu, N. N., M. Alphonse, V. K. Bupesh, S. Shasidhar, T. G. Varun, and R. R. Harinath. 2021. "Experimental Investigation of Hemp Fiber Hybrid Composite Material for Automotive Application." *Materials Today: Proceedings* 44:3666–3672. https://doi.org/10.1016/j.matpr.2020.10.798.

Nadeem, M., H. Jamshaid, R. Mishra, N. Ahmed, V. Chandan, P. Jirku, and V. Kolar. 2023. "Taguchi-TOPSIS Based Optimization of Comfort in Compression Stockings for Vascular Disorders." *Scientific Reports* 13 (1): 15888. https://doi.org/10.1038/s41598-023-43268-7.

Najeeb, M. I., M. T. H. Sultan, A. U. Shah, M. S. M. Amir, S. N. A. Safri, M. Jawaid, and M. R. Shari. 2021. "Low-Velocity Impact Analysis of Pineapple Leaf Fiber (PALF) Hybrid Composites." *Polymers* 13 (18): 31904. https://doi.org/10.3390/polym13183194.

Ng, L. F., M. Y. Yahya, C. Muthukumar, X. J. Woo, A. H. Muhaimin, and R. A. Majid. 2023. "Mechanical Characterization of Aluminum Sandwich Structures with Woven-Ply Pineapple Leaf/Glass Fiber-Reinforced Hybrid Composite Core." *Journal of Natural Fibers* 20 (1): 2160404. https://doi.org/10.1080/15440478.2022.2160404.

Nsengiyumva, W., S. Zhong, J. Lin, Q. Zhang, J. Zhong, and Y. Huang. 2021. "Advances, Limitations and Prospects of Nondestructive Testing and Evaluation of Thick Composites and Sandwich Structures: A State-Of-The-Art Review." *Composite Structures* 256:112951. https://doi.org/10.1016/j.compstruct.2020.112951.

Olhan, S., V. Khatkar, and B. K. Behera. 2022. "Impact Behavior of Long Glass Fibre Reinforced Aluminum Metal Matrix Composite Prepared by Friction Stir Processing Technique for Automotive." *Journal of Composite Materials* 56 (14): 2157–2167. https://doi.org/10.1177/00219983221092012.

Pang, X., W. Yang, W. Miao, H. Zhou, and R. Min. 2024. "Study on Site Selection Evaluation of Emergency Material Storage Based on Improved TOPSIS." *Kybernetes*. https://doi.org/10.1108/K-12-2023-2555.

Pernas-Sánchez, J., S. M. García-Rodríguez, J. A. Artero-Guerrero, J. López-Puente, and J. Costa. 2023. "High Velocity Impact Response of Carbon/Epoxy Composite Laminates at Cryogenic Temperatures." *Composites Part A, Applied Science and Manufacturing* 168:107456. https://doi.org/10.1016/j.compositesa.2023.107456.

Ravi, Y. V., N. Kapilan, S. Rajole, Y. S. Balaji, N. Varun, and B. K. Venkatesha. 2022. "Damage Resistance Evaluation of E-Glass and Hybrid Hemp-Banana Natural Fiber Composite Helmet Using Drop Weight Impact Test." *Materials Today: Proceedings* 54:330–335. https://doi.org/10.1016/j.matpr.2021.09.213.

Sahu, P., and M. Gupta. 2020. "A Review on the Properties of Natural Fibres and Its Bio-Composites: Effect of Alkali Treatment." *Proceedings of the Institution of Mechanical Engineers, Part L: Journal of Materials: Design and Applications* 234 (1): 198–217. https://doi.org/10.1177/1464420719875163.

Sangsefidi, M., H. Sabouri, M. Mir, and A. Hasanpour. 2021. "High-Velocity Impact Response of Fiber Metal Laminates: Experimental Investigation of projectile's Deformability." *Thin-Walled Structures* 159:107169. https://doi.org/10.1016/j.tws.2020.107169.

Selvaraj, R., A. Maneengam, and M. Sathiyamoorthy. 2022. "Characterization of Mechanical and Dynamic Properties of Natural Fiber Reinforced Laminated Composite Multiple-Core Sandwich Plates." *Composite Structures* 284:115141. https://doi.org/10.1016/j.compstruct.2021.115141.

Shahjouei, S., M. R. Barati, and M. Y. Tooski. 2021. "High Velocity Impact Response and Damage Mechanism of an Aluminium/glass-Carbon Fiber/Epoxy Composite Plate Reinforced with Graphene Nano-Plates." *Fibers and Polymers* 22 (2): 480–488. https://doi.org/10.1007/s12221-021-0105-z.

Sharma, A. P., R. Velmurugan, K. Shankar, and S. K. Ha. 2021. "High-Velocity Impact Response of Titanium-Based Fiber Metal Laminates. Part I: Experimental Investigations." *International Journal of Impact Engineering* 152:103845. https://doi.org/10.1016/j.ijimpeng.2021.103845.

Stephen, C., B. Shivamurthy, A. H. I. Mourad, R. Selvam, and M. Mohan. 2022. "Experimental and Finite Element Study on High-Velocity Impact Resistance and Energy Absorption of Hybrid and Non-Hybrid Fabric Reinforced Polymer Composites." *Journal of Materials Research and Technology* 18:5406–5418. https://doi.org/10.1016/j.jmrt.2022.05.007.

Vasiliev, V. V., and E. V. Morozov. 2018. *Advanced Mechanics of Composite Materials and Structures*. Amsterdam: Elsevier.

Vieira, L. M., Y. Dobah, J. C. Santos, T. H. Panzera, R. J. C. Campos, and F. Scarpa. 2022. "Impact Properties of Novel Natural Fibre Metal Laminated Composite Materials." *Applied Sciences* 12 (4): 1869. https://doi.org/10.3390/app12041869.

Vinod, A., M. R. Sanjay, and S. Siengchin. 2023. "Recently Explored Natural Cellulosic Plant Fibers 2018–2022: A Potential Raw Material Resource for Lightweight Composites." *Industrial Crops and Products* 192:116099. https://doi.org/10.1016/j.indcrop.2022.116099.

Wang, W., J. Ge, X. Yu, and H. Li. 2020. "Environmental Fate and Impacts of Microplastics in Soil Ecosystems: Progress and Perspective." *Science of the Total Environment* 708:134841. https://doi.org/10.1016/j.scitotenv.2019.134841.

Xiao, H., M. T. H. Sultan, F. S. Shahar, S. Y. Nayak, N. Yidris, and A. U. M. Shah. 2023. "Development of Hybrid Aluminum/Carbon Fiber/Pineapple Leaf Fiber Laminates Using Vacuum Assisted Resin Transfer Molding (VARTM) for Automotive Applications." *Applied Composite Materials* 31 (2): 561–581. https://doi.org/10.1007/s10443-023-10183-z.

Xiao, H. Y., M. T. H. Sultan, F. S. Shahar, and S. Y. Nayak. 2024. "Mechanical and Viscoelastic Behavior Characterization of Hybrid Aluminum/Carbon Fiber/Pineapple Leaf Fiber Composite via VARTM for Automotive Industry." *Journal of Natural Fibers* 21 (1): 2382874. https://doi.org/10.1080/15440478.2024.2382874.

Zhu, J., Z. Mao, D. Wu, J. Zhou, D. Jiao, W. Shi, and W. Zhu. 2022. "Progress and Trends in Non-Destructive Testing for Thermal Barrier Coatings Based on Infrared Thermography: A Review." *Journal of Nondestructive Evaluation* 41 (3): 49. https://doi.org/10.1007/s10921-022-00880-3.

Zhu, Q., C. Zhang, J. L. Curiel-Sosa, B. T. Quoc, and X. Xu. 2019. "Finite Element Simulation of Damage in Fiber Metal Laminates Under High Velocity Impact by Projectiles with Different Shapes." *Composite Structures* 214:73–82. https://doi.org/10.1016/j.compstruct.2019.02.009.

Zubillaga, L., A. Turon, J. Renart, J. Costa, and P. Linde. 2015. "An Experimental Study on Matrix Crack Induced Delamination in Composite Laminates." *Composite Structures* 127:10–17. https://doi.org/10.1016/j.compstruct.2015.02.077.